Indium Oxide Nanospirals Made of Kinked Nanowires

Guozhen Shen,[†,‡,*] Bo Liang,[†] Xianfu Wang,[†] Po-Chiang Chen,[‡] and Chongwu Zhou[‡,*]

[†]Wuhan National Laboratory for Optoelectronics and College of Optoelectronic Science and Engineering, Huazhong University of Science and Technology, Wuhan 430074, China and [‡]Department of Electrical Engineering, University of Southern California, Los Angeles, California 90089, United States.

ABSTRACT Helical inorganic nanostructures have received great attention due to their unique structures that could be interesting for both fundamental research and nanodevice applications. Using a tube-in-tube laser ablation chemical vapor deposition (CVD) method with gold nanoparticles as the catalysts, we reported the synthesis of self-assembled kinked In_2O_3 nanospirals and multikinked nanowires. As-synthesized nanostructures showed ultrafast photoinduced reversible wettability switching behavior from hydrophobic (132.7°) to superhydrophilic (0°) within 14 min. Single kinked In_2O_3 nanostructure-based field-effect transistors were fabricated, and mobilities higher than 200 $cm^2/(V \cdot s)$ were obtained, revealing good opportunity in fabricating high-performance electronic and optoelectronic devices.

KEYWORDS: nanospirals · kinked · In_2O_3 · nanowires · transistors

Control and modulation of the composition, morphology, doping states, and crystal structures of one-dimensional (1-D) nanostructures during the synthetic process have attracted great interest in recent years[1−7] because they are important for exploring the applications of 1-D nanostructures in various fields, such as electronics, optoelectronics, solar cells, chemical/biosensors, and displays. Recently, helical inorganic nanostructures have received great attention due to their unique structures that could be interesting for both fundamental research and nanodevice applications.[3−10] Helical structures, including nanorings, nanosprings, and nanospirals, have been observed for a number of inorganic materials including carbon nanotubes, ZnO, SnO_2, AlN, SiC, ZnS, $Ag_2V_4O_{11}$,[3−13] *etc*. All of the reported helical nanostructures are composed of smooth nanowires/nanotubes, and kinked nanospirals have not yet reported. Very recently, Lieber's group reported the synthesis of single-crystalline kinked semiconductor nanowires *via* a nanocluster-catalyzed vapor−liquid−solid method.[14] The method is effective for controlling the shapes of the nanostructures. However, it is relatively complicated for large-scale applications, and thus, developing facile and efficient methods to get kinked helical nanostructures is needed.

In this paper, using a tube-in-tube laser ablation chemical vapor deposition (CVD) method with gold nanoparticles as the catalysts, we report the synthesis of self-assembled kinked In_2O_3 nanospirals and multikinked nanowires. The shapes of the as-obtained nanostructures were controlled by the vapor concentrations within the system. Single kinked In_2O_3 nanostructure-based field-effect transistors were fabricated, and mobilities higher than 200 $cm^2/(V \cdot s)$ were obtained, revealing good opportunity in fabricating high performance electronic and optoelectronic devices.

RESULTS AND DISCUSSION

The In_2O_3 nanospirals were synthesized *via* a tube-in-tube laser ablation chemical vapor deposition (CVD) method with gold nanoparticles as the catalysts (Scheme 1). For the synthesis of kinked In_2O_3 nanospirals, a small quartz tube with one end closed was used (Scheme 1a), while a small quartz tube with open ends was used for the synthesis of multikinked In_2O_3 nanowires (Scheme 1b). The composition and structure were checked using X-ray diffraction, and the result indicates the formation of pure In_2O_3 product (Supporting Information, Figure S1). After synthesis, spiral-like nanostructures were found deposited on the whole substrate on a large-scale in the case of using a system containing a small tube with one closed end (Supporting Information, Figure S2). The detailed structure of the product was checked using scanning electron microscopy (SEM), and the results are depicted in Figure 1. Interesting spiral-like structures were found deposited on the silicon substrate with a relatively high yield (Supporting Information, Figure S3). Figure 1b−f shows the SEM images of several

* Address correspondence to gzshen@mail.hust.edu.cn, chongwuz@usc.edu.

Received for review December 7, 2010 and accepted February 10, 2011.

Published online February 17, 2011
10.1021/nn103358y

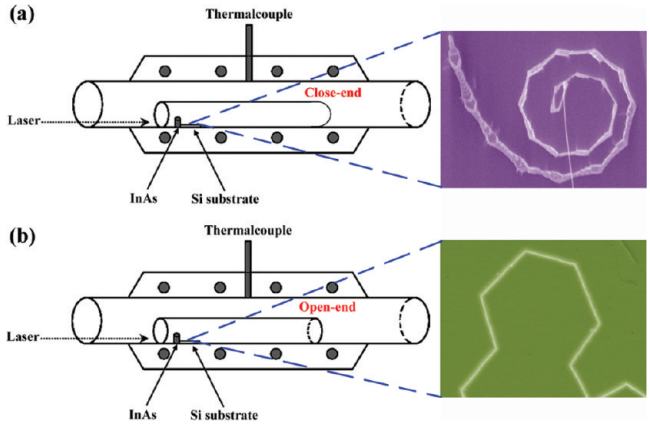

Scheme 1. Schematic illustrations of the tube-in-tube systems designed for the synthesis of (a) kinked In_2O_3 nanospirals and (b) multikinked In_2O_3 nanowires.

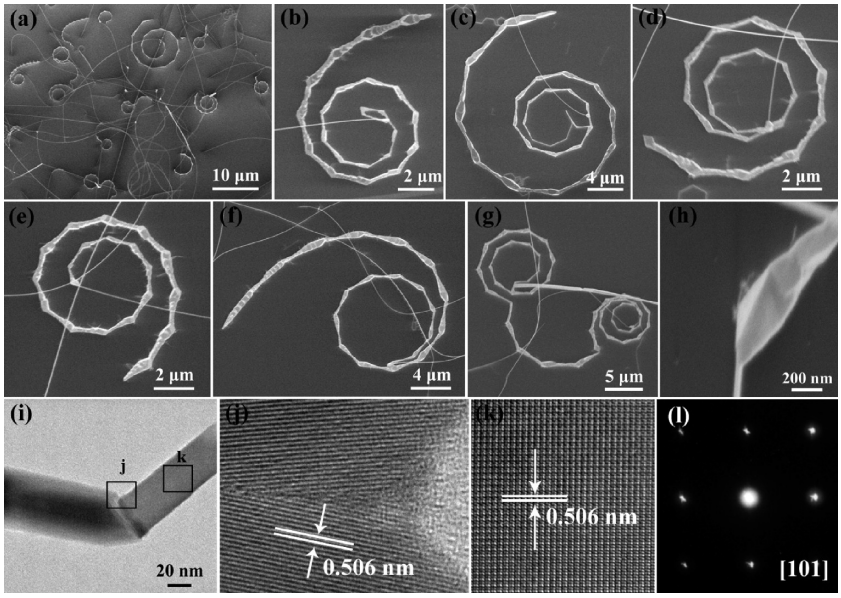

Figure 1. As-grown In_2O_3 nanospirals made by kinked nanowires using the laser ablation CVD process with one end of the tube closed.

nanospirals. The self-coiling of many arm segments resulted in the final kinked nanospirals, which are quite different from all of the previously reported smooth nanospirals. Both the lengths and diameters of the arm segments increased from the core part to the edge part of the nanospirals, also indicated in Figure 1h, which represents as another distinct characteristic compared with previous smooth nanospirals having uniform diameters. Both right-handed (Figure 1b-e) and left-handed (Figure 1f) nanospirals were observed in the products. In some cases, several kinked nanospirals tend to connect with each other, as shown in Figure 1g.

The structure of the nanospirals was characterized by transmission electron microscopy (TEM). The sample was prepared by ultrasonicating the sample in solution and then deposited on a TEM grid. Figure 1i depicts a TEM image of a single kink. Two arms of the kink have different diameters, in good agreement with the SEM results. Lattice-resolved TEM images from the marked regions in panel i of Figure 1 are demonstrated in Figure 1j,k, respectively. Twin defects are clearly seen in the kink part as revealed in Figure 1j. Similar phenomena were frequently observed for modulated nanowires, which may also be applicable here to explain the formation of kink nanostructures.[14−16] As for each arm of the kink, the TEM image shown in Figure 1k confirms its single-crystalline nature. The clearly resolved lattice fringes along/parallel to the growth direction are both 0.506 nm, corresponding to the (020) planes of cubic In_2O_3 phase. A selected area electron diffraction (SAED) pattern along the [001] zone axis taken from the same part is shown in Figure 1l. Along with the TEM image in Figure 1k, it confirms the single-crystalline nature of the arms with the preferred growth directions along the ⟨100⟩ planes.

The composition of the nanospirals was checked using energy-dispersive X-ray spectroscopy (EDS) attached to the TEM. Figure 2 is a typical EDS spectrum taken from a single nanospiral. Only peaks from In and O are observed, indicating the formation of pure In_2O_3 phase. In the spectrum, the peaks from Cu come from the copper grid for TEM analysis. The above results confirm the formation of pure In_2O_3 product, though the target we used was InAs. During the reaction, InAs was ablated and transported by the carrier gases, which was oxidized by the residual in the reaction system to form into In_2O_3 *via* the reaction

$$4InAs + 3O_2 \rightarrow 2In_2O_3 + 4As$$

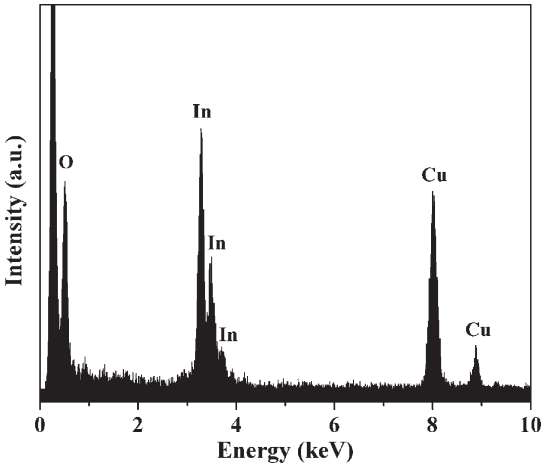

Figure 2. EDS spectrum of the as-synthesized nanospiral, showing the formation of pure In_2O_3.

The Gibbs free energy calculated for the reaction is −1188.6 kJ/mol. The large negative Gibbs free energy indicates that InAs tends to be oxidized into In_2O_3 once trace of oxygen remains in the system at high temperature.

In our experiments, we also observed that, when a small tube with open ends was used instead of a small tube with one closed end, multikinked In_2O_3 nanowires were produced instead of kinked nanospirals. Figure 3 shows the corresponding results of the produced multikinked nanowires. Panels a−d of Figure 3 are the SEM images of several as-synthesized multikinked nanowires, which are found to be composed of many arm segments (Supporting Information, Figure S4). Contrary to the kinked nanospirals with arm segments with varied diameters and lengths, the arm segments of multikinked In_2O_3 nanowires are quite uniform (with a diameter of ∼20 nm) for each kinked nanowire, which can be easily seen from high-magnification SEM images in Figure 3e,f. Figure 3g is a HRTEM image of the junction part between two arm segments. The marked lattice fringes are calculated to be about 0.25 and 0.18 nm, respectively. The values correspond to the (010) and (100) planes of the cubic In_2O_3 phase, indicating that the neighboring two segments of the multikinked In_2O_3 nanowires grow along the ⟨100⟩ and ⟨110⟩ planes, respectively, as marked in Figure 3g. On the image, no clear twin defect was observed, also contrary to the kinked In_2O_3 nanospirals.

Compared to the experimental setup for the synthesis of kinked In_2O_3 nanospirals and multikinked In_2O_3 nanowires, the only difference is the usage of a small

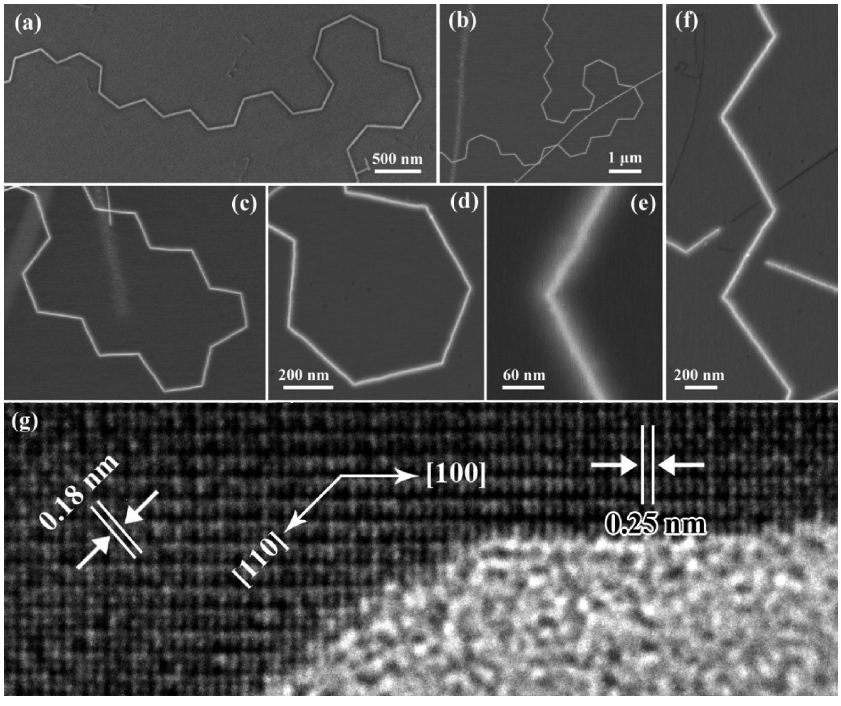

Figure 3. Multikinked In_2O_3 nanowires from the laser ablation CVD process containing a small tube with open ends.

quartz tube with either one closed end or open ends, which resulted in a great difference in vapor concentrations. The vapor concentrations and oxygen partial pressure are known as one of the most important factors that influence the structure and morphology of the synthesized nanostructures, according to previous reports.[16,17] Comparative experiments were carried out in a one-tube laser ablation CVD process to elucidate the effect of vapor concentration on nanostructure growth. While In_2O_3 nanowires were grown under such conditions, the synthesized In_2O_3 nanowires are normal straight nanowires without any kinking (Supporting Information, Figure S5). Kinked nanostructures, nanospirals, and multikinked nanowires can only be obtained under high vapor concentration in the tube-in-tube CVD process.

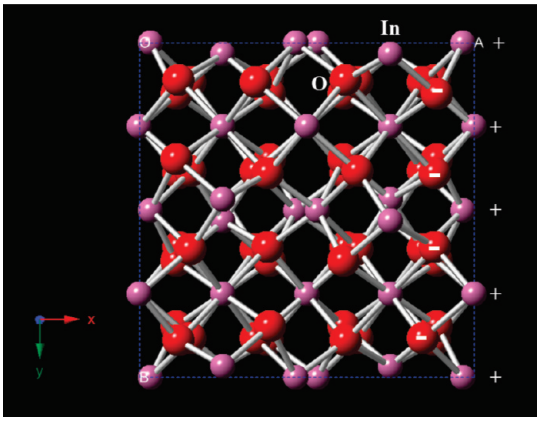

Scheme 2. Schematic illustration of the structure model of an In_2O_3 lattice projected along the [001] orientation, displaying ±(100) polar surfaces.

As for the growth of inorganic nanospirals, the polar surfaces existing within the material lattice have been widely used to explain their growth mechanism. For example, Wang *et al.* synthesized rutile-structured SnO_2 nanospirals, and the ±(011) polar surfaces were thought to be the main formation mechanism.[9] Recently, a fancy work was done by Wu *et al.*, where they observed the first $CrSi_2$ hexagonal nanowebs.[18] The surface charges and the minimization of electrostatic energy were the dominant growth mechanism. From the structure analysis shown in Figures 2, all segments of our In_2O_3 nanospirals have the growth direction along the ⟨100⟩ planes. The side surfaces are (010) and (100) planes. Shown in Scheme 2 is a structure model of an In_2O_3 lattice projected along the [001] orientation. From the image, we can see that, when grown along the ⟨100⟩ planes, the ±(100) surfaces are In^{3+} and O^{2-} terminated polar surfaces. Thus, a similar polar surface induced growth mechanism was proposed for the formation of kinked In_2O_3 nanospirals. As for the multikinked In_2O_3 nanowires, the growth directions were found to switch between ⟨100⟩ and ⟨110⟩, as indicated in Figure 3g. The switch in growth direction from [110] to [100], which is 45°, for example, results in the multikinked structure. The growth of multikinked nanowires in Figure 3 may not be simply explained from the polar surface view. As indicated above, the ±(100) surfaces

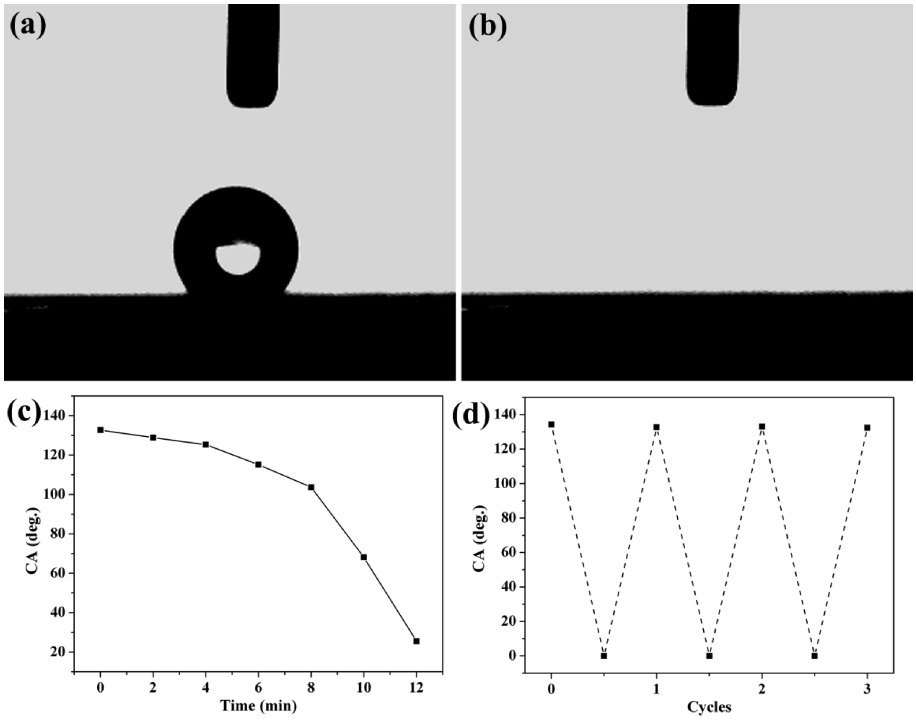

Figure 4. Photoinduced reversible wettability of multikinked In_2O_3 nanowires. (a) Before and (b) after UV illumination. (c) Gradually decreasing water contact angles under UV illumination. (d) Reversible wettability conversions *via* UV illumination and dark storage.

are In^{3+} and O^{2-} terminated polar surfaces when grown along the ⟨100⟩ planes, while the side surfaces are nonpolar surfaces that grew along the ⟨110⟩ planes. In this case, the variation of vapor transport rate and the partial pressure of the reaction species should be also considered to explain the possible growth mechanism. As indicated by Wu *et al.*, in the vapor phase synthesis, the surface reconstruction may lead to charged surfaces.[18] The exact mechanism remains as open questions and more experimental and theoretical work are still underway in our group.

We now examine the interesting properties of the as-synthesized nanomaterials on the substrate surface. The wetting behavior of solid surfaces is ubiquitous and has attracted great interests in recent years when combined with the fast expanding nanotechnology.[19−25] Wettability in terms of contact angle (CA), one of the most important properties of a solid surface, is thought to be governed by two factors: the chemical composition and the roughness of the surface. The surface wettability of the as-synthesized multikinked In_2O_3 nanowires was studied by measuring the contact angle, and the results are shown in Figure 4. A water droplet shape on the nanowire films is depicted in Figure 4a, revealing the CA of 132.7°. The CA is much larger than In_2O_3 films with smooth surfaces, where the CA is around 20°,[24] and is comparable with the CA of high density In_2O_3 nanowire arrays (155°).[25] More than 10 samples were checked, and they all give similar CA values in the range of 130−134°. According to previous reports, the surface roughness of nanostructures contained enough room to hold air in the troughs between nanowires.[22] Similar mechanism was also applied to the multikinked In_2O_3 nanowires here.

When the films are exposed to UV light with a wavelength of 254 nm, the CA gradually decreased with the increase of exposing time, as indicated in Figure 4c. After being exposed for 14 min, the CA was observed to be around 0° (Figure 4b), showing the photoinduced conversion of the surface wettability from hydrophobic (132.7°) to superhydrophilic (0°). It is known that, when nanowire films are exposed to UV light, electron−hole pairs will be generated on the surface of the multikinked In_2O_3 nanowires. Some of the holes then oxidize lattice oxygen to dissociative oxygen, resulting in the formation of oxygen vacancies on the nanowires' surface. Compared with oxygen molecules in air, water molecules are more favored by the defective sites because of the strong adsorption between oxygen vacancy and hydroxyl, which leads to a hydrophilic In_2O_3 nanowire film.[19−21] The transition rate measured here is ∼30 times faster than the previously reported behavior of aligned In_2O_3 nanowire arrays, where it took 6 h for the sample to change from 155 to 20°.[25] Compared to the aligned In_2O_3 nanowire arrays with diameters of ∼100 nm, our multikinked nanowires have much smaller diameters (∼20 nm), which means larger surface area. Furthermore, our nanowires here have good single crystallinity and low defect density. Once exposed to UV irradiation, more electron−hole pairs are generated, resulting in much more oxygen vacancies on the surface. Thus, much faster conversion of surface wettability was obtained. Similar results were also reported for ZnO nanostructures, TiO_2, and so on.[26]

After UV exposure, the exposed multikinked In_2O_3 nanowires were stored in the dark for several days and it was found that the wettability returns to hydrophobic again and the cycles can be repeated, as revealed in Figure 4d. The phenomena can be explained by the replacement of adsorbed hydroxyls by oxygen in air since oxygen adsorption is thermodynamically more stable.[19−21] It makes the surfaces of the In_2O_3 nanowires return to the initial state and the wettability of the films reconverts to hydrophobicity.

As an important wide band gap transparent semiconductor, In_2O_3 has great applications in electronic and optoelectronic devices, such as transparent electronics, solar cells, light-emitting diodes, and gas sensors, *etc.*[27−30] Here, we fabricated single nanostructure-based FETs directly on the grown Si/SiO_2 substrate to investigate the electric transport properties of our kinked In_2O_3 nanostructures. Briefly, the silicon substrate with grown In_2O_3 nanostructures was cleaned with ethanol several times and dried for use. Photolithography was then performed with a designed mask, followed by Ti/Au deposition to pattern the source and drain electrodes on both ends of the nanowires. The thickness of Ti is 5 nm and that of Au is 95 nm.

The inset of Figure 5a is a schematic illustration of a typical device, and a SEM image of the single nanowire device was shown in the inset of Figure 5b. Figure 5a is the drain current (I_{DS}) *versus* source-drain voltage (V_{DS}) curves of a typical device. Linear current *versus* voltage is obtained, indicating very good Ohmic contacts. From the curves, it can be seen that the conductance increases gradually with increased gate voltage ranging from −40 to 40 V, indicating typical n-type semiconducting behaviors. The $I_{DS}-V_G$ curve was also measured for the same device, and the result is shown in Figure 5b, which also implies that kinked In_2O_3 nanostructures are n-type semiconductors. The transconductance values, g_m, derived from the equation $g_m = dI/dV_G$, can be calculated from the linear region of V_G shown in Figure 5b. The transconductance g_m is calculated to be 5.1 nA/V. The electron mobility was calculated from the equation $g_m = \mu(C/L^2)V_{DS}$, where μ is the mobility, L is the nanowire channel length, and C is the capacitance of the back gate and can be estimated from $C \approx 2\pi\varepsilon\varepsilon_o L/\ln(2h/r)$, where h is the thickness of the silicon dioxide layer, ε is the dielectric constant of silicon dioxide. On the basis of the above equations, the mobility was calculated to be around 243 $cm^2/(V\cdot s)$.

Single nanowire FETs were also fabricated by using the synthesized kinked In_2O_3 nanospirals, and the

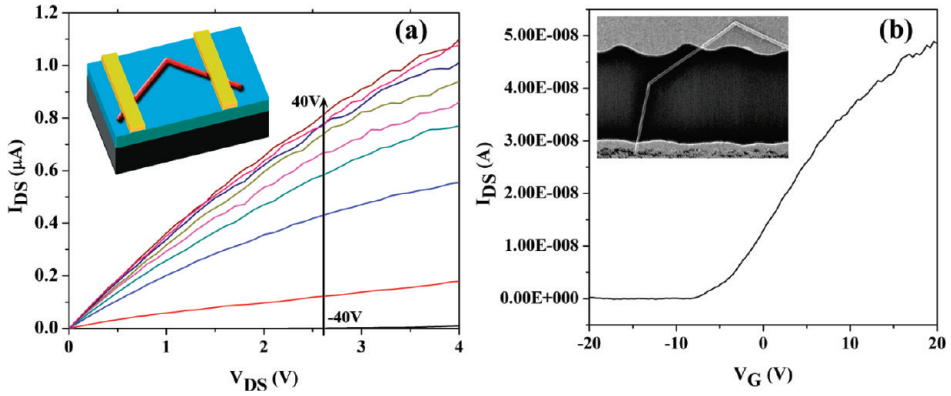

Figure 5. Current−voltage data recorded from a FET built on a single kinked In_2O_3 nanowire. (a) $I_{DS}-V_{DS}$ curves measured at different gate voltages with a step of 5 V. (b) $I_{DS}-V_G$ transfer curves. Inset in panel b is a SEM image of the fabricated device.

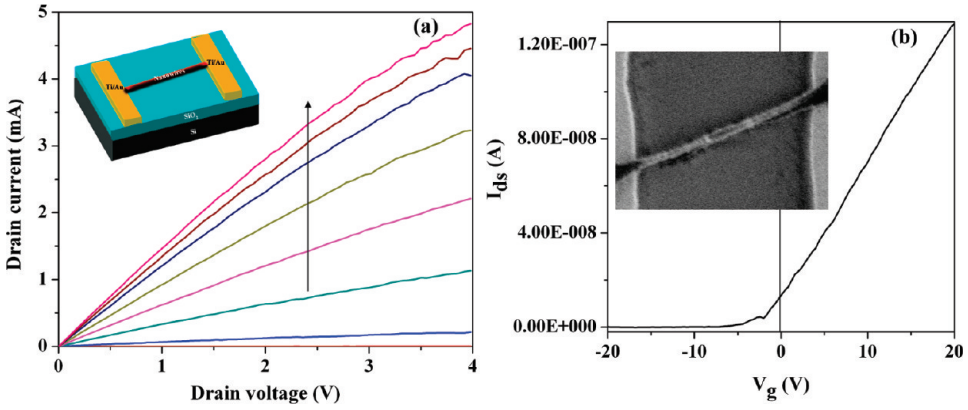

Figure 6. Current−voltage data recorded from a FET built on a single kinked In_2O_3 nanospiral. (a) $I_{DS}-V_{DS}$ curves measured at different gat voltages with a step of 5 V. The arrow indicates the variation of gate voltages from −40 to 40 V. (b) $I_{DS}-V_G$ transfer curves. Inset in panel b is a SEM image of the fabricated device.

corresponding electronic transport data are shown in Figure 6. A SEM image of the device is depicted in the inset of Figure 6b, where the device channel is around 1.5 μm and the diameter of the nanowire is around 50 nm. Figure 6a is the drain current (I_{DS}) *versus* source-drain voltage (V_{DS}) curves of a typical device. Linear current *versus* voltage is also obtained as shown in the image, indicating very good Ohmic contacts. From the curves, we can see that kinked In_2O_3 nanospirals are typical n-type semiconductors. The device mobility was calculated according to $g_m = \mu(C/L^2)V_{DS}$ and is around 207 $cm^2/(V \cdot s)$. This value is comparable to conventional In_2O_3 nanowire FETs, indicating its potential application in fabricating high-performance electronic and optoelectronic devices.

In summary, we succeeded in synthesizing kinked In_2O_3 nanospirals and multikinked nanowires *via* a tube-in-tube laser ablation CVD method. The as-synthesized multikinked nanowires show hydrophobic wettability with a CA of 132.7° and ultrafast photoinduced reversible switching behavior. Single nanostructure-based FETs were fabricated, and the results indicate that they are good candidates for fabricating high-performance electronic and optoelectronic devices. Fundamentally, such method can be expanded to synthesize other inorganic nanostructures with interesting shapes.

EXPERIMENTAL SECTION

In a typical process, a thin layer of gold nanoparticles with diameters of 20 ± 2.0 nm (Ted Pella) were coated on the substrate as the catalysts for nanostructure growth. The silicon substrate was loaded into the downstream part of a small quartz tube, which was put into a 2.5 in. quartz tube of a furnace. An InAs (Alfa Aesar, 99.999%) target was then placed at the upper entrance part of the small quartz tube. The system was first pumped to a base pressure below 1 mTorr to eliminate oxygen in the reaction system, and then pure Ar (99.999%) was flown through the system at a rate of 100 sccm. A pulsed Nd:YAG laser with repetition rate of 10 Hz and a pulse power of 1.0 W was used. During the laser ablation process, the chamber was maintained at 750 °C under atmospheric pressure, and the

reaction time was 1 h. After synthesis, a layer of white product was found deposited on the substrate.

The structure and composition of the products were characterized using X-ray diffraction (RINT 2200). Scanning electron microscopy (SEM) was performed on a Hitachi field-emission SEM (S-4800). The microstructures of the synthesized products were checked using a transmission electron microscope (JEOL 2100). The surface wettability was investigated by measuring the water contact angle by an SL200B contact angle system (Solon Technology Science Co., Ltd.) at ambient pressure and room temperature.

Acknowledgment. This work was supported by National Natural Science Foundation of China (51002059), the 973 Projects of China (2011CBA00700), the Natural Science Foundation of Hubei Province (2009CDB326), and the Research Fund for the Doctoral Program of Higher Education (20090142120059). We express our deep thanks to Prof. Zhong Lin Wang of Georgia Institute of Technology for his careful supervision, strong support, and stimulating discussion, especially on the microstructure analysis, growth mechanism, and English editing.

Supporting Information Available: X-ray diffraction pattern of the In_2O_3 product, optical image of the synthesized kinked In_2O_3 nanospirals, low-magnification SEM images of the synthesized kinked In_2O_3 nanospirals, low-magnification SEM images of the synthesized multikinked In_2O_3 nanowires, and SEM image of straight In_2O_3 nanowires obtained in a normal laser ablation CVD process. This material is available free of charge *via* the Internet at http://pubs.acs.org.

REFERENCES AND NOTES

1. Gudiksen, M. S.; Lauhon, L. J.; Wang, L.; Smith, D. C.; Lieber, C. M. Growth of Nanowire Superlattice Structures for Nanoscale Photonics and Electronics. *Nature* **2002,** *415*, 617–620.
2. Amelinekx, S.; Zhang, X. B.; Bernacrts, D.; Zhang, X. F.; Ivanov, V.; Nagy, J. B. A Formation Mechanism for Catalytically Grown Helix-Shaped Graphite Nanotubes. *Science* **1994,** *265*, 635–639.
3. Kong, X. Y.; Wang, Z. L. Spontaneous Polarization-Induced Nanohelixes, Nanosprings, and Nanorings of Piezoelectric Nanobelts. *Nano Lett.* **2003,** *3*, 1625–1631.
4. Zhang, J.; Chen, P. C.; Shen, G. Z.; He, J.; Kumbhar, A.; Zhou, C.; Fang, J. p-Type Field-Effect Transistors of Single-Crystal ZnTe Nanobelts. *Angew. Chem., Int. Ed.* **2008,** *47*, 9469–9471.
5. Lu, W.; Gao, P.; Jian, W. B.; Wang, Z. L.; Fang, J. Perfect Orientation Ordered *In-Situ* One-Dimensional Self-Assembly of Mn-Doped PbSe Nanocrystals. *J. Am. Chem. Soc.* **2004,** *126*, 14816–14821.
6. Wang, X. D.; Song, J.; Liu, J.; Wang, Z. L. Direct-Current Nanogenerator Driven by Ultrasonic Waves. *Science* **2007,** *316*, 102–105.
7. Kong, X. Y.; Ding, Y.; Yang, R.; Wang, Z. L. Single-Crystal Nanorings Formed by Epitaxial Self-Coiling of Polar Nanobelts. *Science* **2004,** *303*, 1348–1351.
8. Gao, P. X.; Ding, Y.; Mai, W.; Hughes, W. L.; Lao, C.; Wang, Z. L. Conversion of Zinc Oxide Nanobelts into Superlattice Structured Nanohelices. *Science* **2005,** *309*, 1700–1704.
9. Yang, R. S.; Wang, Z. L. Springs, Rings, and Spirals of Rutile-Structured Tin Oxide Nanobelts. *J. Am. Chem. Soc.* **2006,** *128*, 1466–1467.
10. Duan, J.; Yang, S.; Liu, H.; Gong, J.; Huang, H.; Zhao, X.; Tang, J.; Zhang, R.; Du, Y. AlN Nanorings. *J. Cryst. Growth* **2005,** *283*, 291–296.
11. Shen, G. Z.; Chen, D. Self-Coiling of $Ag_2V_4O_{11}$ Nanobelts into Perfect Nanorings and Microloops. *J. Am. Chem. Soc.* **2006,** *128*, 11762–11763.
12. Shen, G. Z.; Bando, Y.; Zhi, C.; Yuan, X.; Sekiguchi, T.; Golberg, D. Single-Crystalline Cubic Structured InP Nanosprings. *Appl. Phys. Lett.* **2006,** *88*, 243106.
13. Zhang, H.; Wang, C. M.; Wang, L. S. Helical Crystalline SiC/SiO_2 Core−Shell Nanowires. *Nano Lett.* **2002,** *2*, 941–944.
14. Tian, B.; Xie, P.; Kempa, T. J.; Bell, D. C.; Lieber, C. M. Single-Crystalline Kinked Semiconductor Nanowire Superstructures. *Nat. Nanotechnol.* **2009,** *4*, 824–829.
15. Algra, R. E.; Verheijen, M. A.; Borgstrom, M. T.; Feiner, L. F.; Immink, G.; van Enckevort, W. J. P.; Vlieg, E.; Bakkers, E. P. A. M. Twinning Superlattices in Indium Phosphide Nanowires. *Nature* **2008,** *456*, 369–372.
16. Caroff, P.; Dick, K. A.; Johansson, J.; Messing, M. E.; Deppert, K.; Samuelson, L. Controlled Polytypic and Twin-Plane Superlattices in III−V Nanowires. *Nat. Nanotechnol.* **2009,** *4*, 50–55.
17. Shen, G. Z.; Chen, P. C.; Bando, Y.; Golberg, D.; Zhou, C. W. Single-Crystalline and Twinned Zn_3P_2 Nanowires: Synthesis, Characterization and Electronic Properties. *J. Phys. Chem. C* **2008,** *112*, 16405–16410.
18. Wang, H. T.; Wu, J. C.; Shen, Y. Q.; Li, G. P.; Zhang, Z.; Xing, G. Z.; Guo, D. L.; Wang, D. D.; Dong, Z. L.; Wu, T. $CrSi_2$ Hexagonal Nanowebs. *J. Am. Chem. Soc.* **2010,** *132*, 15875–15877.
19. Zhu, W. Q.; Feng, X. J.; Feng, L.; Jiang, L. UV-Manipulated Wettability between Superhydrophobicity and Superhydrophilicity on a Transparent and Conductive SnO_2 Nanorod Film. *Chem. Commun.* **2006,** 2753–2755.
20. Chen, A. C.; Peng, X. S.; Koczkur, K.; Miller, B. Super-Hydrophobic Tin Oxide Nanoflowers. *Chem. Commun.* **2004,** 1964–1966.
21. Chang, F. M.; Cheng, S. L.; Hong, S. J.; Sheng, Y. J.; Tsao, H. K. Superhydrophilicity to Superhydrophobicity Transition of CuO Nanowire Films. *Appl. Phys. Lett.* **2010,** *96*, 114101.
22. Niu, J. J.; Wang, J. N. Direct Synthesis of Superhydrophobic Silica Nanowires Surface by Evaporating ZnS on Silicon Wafer. *Cryst. Growth Des.* **2008,** *8*, 2793–2798.
23. Yan, B.; Tao, J.; Pang, C.; Zheng, Z.; Shen, Z.; Alfred Huan, C. H.; Yu, T. Reversible UV-Light-Induced Ultrahydrophobic-to-Ultrahydrophilic Transition in an α-Fe_2O_3 Nanoflakes Film. *Langmuir* **2008,** *24*, 10569–10571.
24. Miyauchi, M.; Nakajima, A.; Watanabe, T.; Hashimoto, K. Photocatalysis and Photoinduced Hydrophilicity of Various Metal Oxide Thin Films. *Chem. Mater.* **2002,** *14*, 2812–2816.
25. Zhong, M.; Zheng, M.; Zeng, A.; Ma, L. Direct Integration of Vertical In_2O_3 Nanowire Arrays, Nanosheet Chains, and Photoinduced Reversible Switching of Wettability. *Appl. Phys. Lett.* **2008,** *92*, 093118.
26. Zhang, Z.; Chen, H.; Zhong, J.; Saraf, G.; Lu, Y. Fast and Reversible Wettability Transitions on ZnO Nanostructures. *J. Electron. Mater.* **2007,** *36*, 895–899.
27. Zhang, D.; Liu, Z.; Li, C.; Tang, T.; Liu, X.; Han, S.; Lei, B.; Zhou, C. Detection of NO_2 Down to ppb Levels Using Individual and Multiple In_2O_3 Nanowire Devices. *Nano Lett.* **2004,** *4*, 1919–1924.
28. Liang, C.; Meng, G. W.; Lei, Y.; Phillipp, F.; Zhang, L. D. Catalytic Growth of Semiconducting In_2O_3 Nanofibers. *Adv. Mater.* **2001,** *13*, 1330–1333.
29. Lao, J.; Huang, J.; Wang, D. Z.; Ren, Z. F. Self-Assembled In_2O_3 Nanocrystal Chains and Nanowire Networks. *Adv. Mater.* **2004,** *16*, 65–69.
30. Yu, J.; Wang, Y.; Wen, W.; Yang, D.; Huang, B.; Li, J.; Wu, K. Aluminothermal Reaction Approach for Micro-/Nanofabrications: Syntheses of In_2O_3 Micro-/Nanostructures and InN Octahedral Nanoshells. *Adv. Mater.* **2010,** *22*, 1479–1483.